Rapidity Dependence of Net–protons at $\sqrt{s_{NN}} = 200$ GeV

P. Christiansen[a], for the BRAHMS collaboration

[a]Niels Bohr Institute, University of Copenhagen, Denmark

The BRAHMS collaboration has measured inclusive proton and anti–proton spectra at several rapidities ($0 \leq y \leq 3$) for Au+Au collisions at $\sqrt{s_{NN}} = 200$ GeV. Rapidity densities of protons, anti–protons, and net–protons $[N(p) - N(\bar{p})]$ are presented as a function of rapidity.

1. INTRODUCTION

In his article from 1983 [1], Bjorken proposed a scenario for the evolution of the central rapidity region in ultra relativistic heavy ion collisions. Two of his assumptions were motivated by what had been observed in nucleon-nucleon collisions [2]. First, the collision has to be transparent, meaning that the net–baryon $[N(B) - N(\bar{B})]$ content ends up at forward rapidities after the collision. The second assumption is the existence of a central rapidity plateau with uniform particle production i.e., the invariant yields dN/dy are constant as a function of rapidity (boost invariance). These assumptions allow this region to be described as many identical thermal sources with different longitudinal velocities undergoing only 1–dimensional longitudinal hydrodynamical evolution. In this scenario the initial energy density can be related in a simple way to the final particle production (used in fx. [3]).

At AGS and SPS where the degree of transparency is low, the original baryons are stopped in the initial collisions and the mid–rapidity region contains most of the net–baryons. The measured ratio of anti–protons to protons at the Relativistic Heavy Ion Collider (RHIC) at $\sqrt{s_{NN}} = 200$ GeV, $N(\bar{p})/N(p) \approx 0.75$ ($y = 0$) [4,5], indicates that particle production in the central rapidity region is dominated by pair production.

The BRAHMS experiment at RHIC consists of two magnetic spectrometers with small solid angle coverage. The Mid Rapidity Spectrometer (MRS) ($30° < \theta < 95°$) uses Time-Of-Flight (TOF) for particle identification (PID). In the Forward Spectrometer (FS) ($2.3° < \theta < 30°$) only the Ring Imaging Cherenkov (RICH) is used in this analysis. The experiment is described in full detail in [6]. By combining many different magnet and angle settings, BRAHMS has a wide rapidity coverage for pions, kaons, and protons, that allows the study of boost invariance and transparency at RHIC.

2. RESULTS

For all the data presented here, an event centrality cut of 0–10% ($b \leq 4.4$ fm) was applied. In the MRS, protons and anti–protons are identified using cuts in the mass
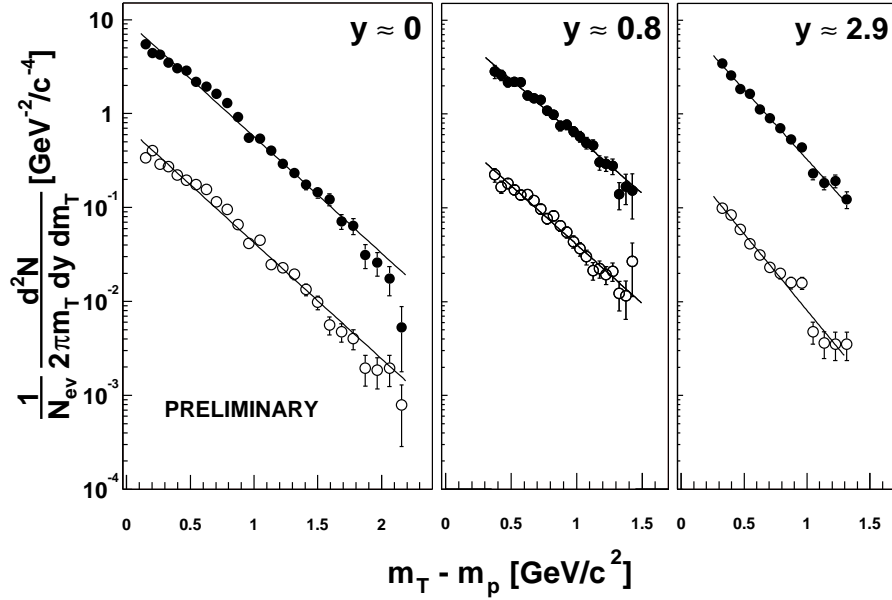
Figure 1. Transverse mass spectra for proton ($\bullet$) and anti–protons ($\circ$). The anti–proton spectra have been divided by a factor of 10 for clarity. Error bars are statistical only. The spectra have been fitted with Eq. 1.

squared m^2 calculated from TOF and momentum p. In the FS, the RICH cannot directly identify protons with momentum $p < 15$ GeV/c. Most of the protons in the settings used here ($y \sim 2.9$) are below that threshold. Instead, the RICH is used to veto pions and kaons. The PID and data selection is described more thoroughly in [5].

For each magnet and angle setting the geometrical acceptance is calculated using a Monte Carlo simulation of the BRAHMS detector. The corrections for multiple scattering and absorption have been calculated in the same simulation framework. Tracking efficiencies for each chamber have been calculated from the data by comparing the number of identified track segments in the chamber to the number of reference tracks determined by other detectors disregarding the chamber under consideration. For the spectrometers the total tracking efficiencies are $\sim 92\%$ in the MRS and $\sim 60\%$ in the FS in the settings used here. After all the corrections have been applied to the data the differential yields are finally projected to the m_T-axis in a narrow rapidity range. Figure 1 shows transverse mass spectra for p and $\bar{p}$ at $y = 0.0, 0.8, 2.9$.

To find the yields dN/dy, the data is fitted with an exponential function (Eq. 1). The fit is used to extrapolate the yields to the regions where there is no data (mainly low m_T).

$$\frac{1}{N_{ev}} \frac{d^2N}{2\pi m_T dy dm_T} = \frac{1}{2\pi} \frac{dN}{dy} \frac{1}{T(T + m_p)} \exp\left(-\frac{m_T - m_p}{T}\right), \tag{1}$$

where m_p is the proton mass, $m_T = \sqrt{p_T^2 + m_p^2}$ is the transverse mass, and T is the effective temperature (inverse slope).

The fit to the data are shown in Fig. 1. The χ^2/DOF is ~ 3–4 for the mid–rapidity data, and ~ 0.75–1.6 at the two forward rapidities. The effective temperature from the fits are the same for protons and anti–protons within 30 MeV. Fig. 2 shows the rapidity dependence of the effective temperature for positive pions, kaons, and protons (pions and
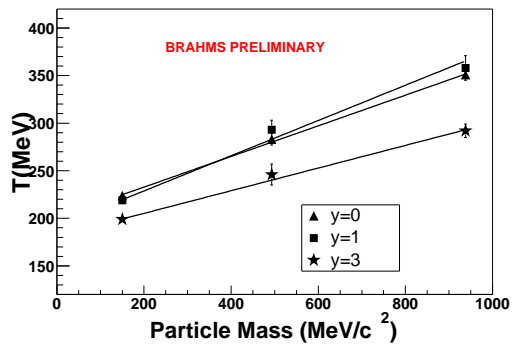
Figure 2. Effective temperatures obtained from fits to pion, kaon, and proton spectra. The solid lines connect data points from the same rapidity.
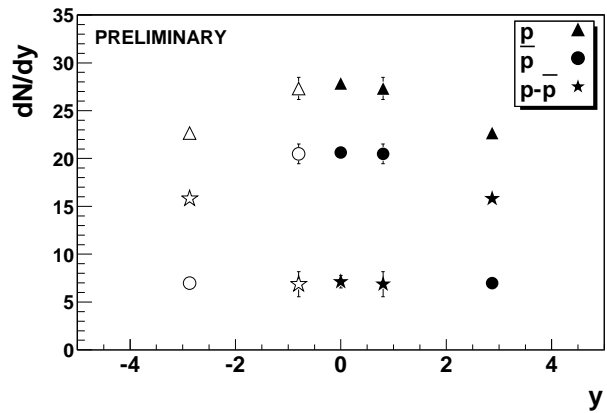
Figure 3. Proton, anti–proton, and net–proton yields as a function of rapidity. Event centrality is 0-10%. Error bars are statistical only.

kaons are from [7]). The mass dependence of the effective temperature is due to strong transverse flow which has a stronger effect on heavier particles. The fact that the effective temperature drops moderately as a function of rapidity indicates that there is strong longitudinal flow, whereas in a thermal isotropic fireball picture the effective temperature drops as $T(y) = T(y = 0)/\cosh(y)$. This would decrease the effective temperature by 90% from $y = 0$ to $y = 2.9$ compared with $\sim 10-20\%$ observed. The effective temperature obtained from the fit is very sensitive to the fit–range used and have a systematic error of 10–15%.

The rapidity dependence of the extrapolated yields, dN/dy, for protons, anti–protons, and net–protons are presented in Fig. 3. The width of the proton distribution is wider than the anti–proton distribution and decreases less than 20% from mid–rapidity to rapidity $y = 3$, whereas pions decrease by 50% [7]. The net–proton distribution increases at forward rapidities where the original baryon content is recovered.

The current systematic errors on the yields are estimated to be 15% in the MRS ($y < 1$) and 20% in the FS. The largest contribution comes from the extrapolation to the yield dN/dy. This effect should not change the shape of the distribution, only the overall level. The systematic error from point to point in rapidity is 10%.

3. DISCUSSION

The yields of pions, kaons, and protons drop less than 10% over the first unit of rapidity. Because of the systematic error, it is premature to rule out or confirm that there is a boost invariant plateau of width $\Delta y \sim 2-3$ rapidity units around mid–rapidity. From the charge conjugate ratios [5] it is clear that it cannot be broader.

Assuming that the anti–proton yields decrease smoothly between rapidity 1 and 3, we can deduce from measurements of the rapidity dependence of $N(\bar{p})/N(p)$ ratio [5] that the proton distribution behaves smoothly in the same interval, so the net–proton distribution does not peak for $y < 3$ i.e., the bulk part of the net–protons is found far from mid–rapidity.
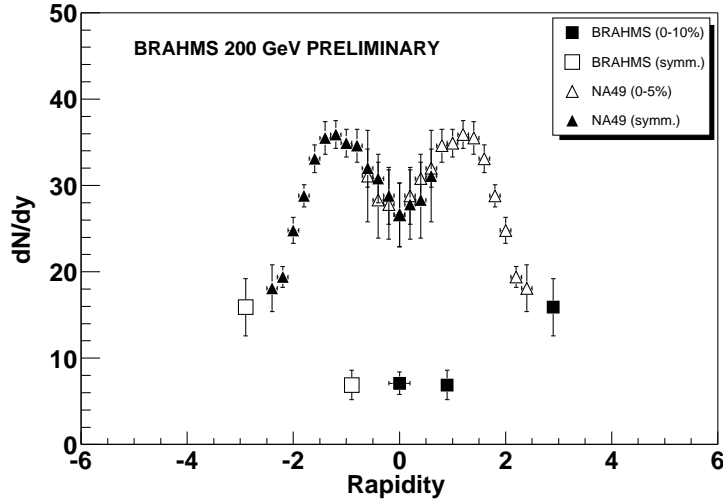
Figure 4. Comparison between net–protons measured at RHIC and SPS [8]. Note that at SPS, $y_{beam} \sim 2.9$ whereas at RHIC $y_{beam} \sim 5.4$. The error bars are statistical and systematic.

When compared to SPS data ($\sqrt{s_{NN}} = 17$ GeV) in Fig. 4, it is clear that the net–proton yield at RHIC is significantly lower (60–70%). At SPS most of the protons at mid–rapidity are net–protons, while at RHIC the pair production mechanism dominates the proton production in the central region and the bulk of the net–protons are found at forward rapidities.

The BRAHMS results shows that the longitudinal flow in the collisions is strong. The proton and anti–proton yields exhibit little variation over at least the 2 central units of rapidity. The BRAHMS data suggest the onset of a boost invariant like plateau around mid–rapidity. The net–proton content of the central rapidity region is much lower than what was observed at lower beam energies, indicating that at RHIC collisions are highly transparent.

REFERENCES

1. J.D. Bjorken, Phys. Rev. D 27 (1983) 140.
2. F. Videbæk and O. Hansen, Phys. Rev. C 52, 2684 and UA5 Collaboration, K. Alpgård et al., Phys. Lett. B 107, 310
3. H. Ito, BRAHMS Collaboration, this proceedings.
4. PHOBOS Collaboration, Submitted to Phys. Rev. C Rapid Comm., nucl-ex/0206012 (2002).
5. BRAHMS Collaboration, Submitted to Phys. Rev. Lett., nucl-ex/0207006 (2002).
6. BRAHMS Collaboration, To be published in Nucl. Instr. Meth.
7. J.I. Jordre, BRAHMS Collaboration, this proceedings. See also I.G. Bearden, J.H. Lee, D. Ouerdane, BRAHMS Collaboration, QM02 proceedings to be published in Nucl. Phys. A.
8. NA49 Collaboration, H. Appelhäuser et al., Phys. Rev. Lett. 82 (1999) 2471.